Regional and global temperature response to anthropogenic SO2 emissions from China in three climate models

Atmos. Chem. Phys. Discuss., doi:10.5194/acp-2015-1017, 2016
Manuscript under review for journal Atmos. Chem. Phys.
Published: 18 January 2016

Atmospheric Chemistry and Physics Discussions

Regional and global climate response to anthropogenic SO_2 emissions from China in three climate models

M. Kasoar[1], A. Voulgarakis[1], J.-F. Lamarque[2], D. T. Shindell[3], N. Bellouin[4], W. J. Collins[4], G. Faluvegi[5], and K. Tsigaridis[5]

[1]{Department of Physics, Imperial College London, London, UK}

[2]{NCAR Earth System Laboratory, National Center for Atmospheric Research, Boulder, CO, USA}

[3]{Nicholas School of the Environment, Duke University, Durham, NC, USA}

[4]{Department of Meteorology, University of Reading, Reading, UK}

[5]{Center for Climate Systems Research, Columbia University, and NASA Goddard Institute for Space Studies, New York, NY, USA}

Correspondence to: M. Kasoar (m.kasoar12@imperial.ac.uk)

Abstract

We use the HadGEM3-GA4, CESM1, and GISS ModelE2 climate models to investigate the global and regional aerosol burden, radiative flux, and surface temperature responses to removing anthropogenic sulfur dioxide (SO_2) emissions from China. We find that the models differ by up to a factor of six in the simulated change in aerosol optical depth (AOD) and shortwave radiative flux over China that results from reduced sulfate aerosol, leading to a large range of magnitudes in the regional and global temperature responses. Two of the three models simulate a near-ubiquitous hemispheric warming due to the regional SO_2 removal, with similarities in the local and remote pattern of response, but overall with a substantially different magnitude. The third model simulates almost no significant temperature response. We attribute the discrepancies in the response to a combination of substantial differences in the chemical conversion of SO_2 to sulfate, translation of sulfate mass into AOD, and differences in the radiative forcing efficiency of sulfate aerosol in the models. The model with the strongest response (HadGEM3-GA4) compares best with observations of AOD

Atmos. Chem. Phys. Discuss., doi:10.5194/acp-2015-1017, 2016
Manuscript under review for journal Atmos. Chem. Phys.
Published: 18 January 2016

regionally, however the other two models compare similarly (albeit poorly) and still disagree substantially in their simulated climate response, indicating that total AOD observations are far from sufficient to determine which model response is more plausible. Our results highlight that there remains a large uncertainty in the representation of both aerosol chemistry as well as direct and indirect aerosol radiative effects in current climate models, and reinforces that caution must be applied when interpreting the results of single-model studies of aerosol influences on climate. Model studies that implicate aerosols in climate responses should ideally explore a range of radiative forcing strengths representative of this uncertainty, in addition to thoroughly evaluating the models used against observations.

1 Introduction

Short-lived atmospheric pollutants such as aerosols have very inhomogeneous spatial distributions. This means that, unlike long-lived greenhouse gases such as CO_2, the radiative forcing due to aerosols is highly variable, and the resulting climate response may be strongly influenced by the region of emission and the prevailing circulation patterns. There is increasing interest in trying to understand how aerosol forcing from different regions affects the climate, both locally and remotely. For example, Shindell and Faluvegi (2009) and Shindell et al. (2012) looked systematically at the response of temperature and precipitation to single-species forcings imposed in different latitude bands, and showed that the influence of remote forcings on certain regions can often outweigh and even have opposite sign to the influence of local forcings. Teng et al. (2012) investigated the global temperature response to drastically increasing carbonaceous aerosols only over Asia, finding a strong remote effect on US summertime temperatures.

One of the most important anthropogenically-sourced aerosol species is sulfate (SO_4) (e.g. Myhre et al., 2013b). Sulfate-containing aerosols are formed following chemical conversion of gaseous sulfur dioxide (SO_2) emissions from fossil-fuel combustion, as well as natural sources such as volcanic SO_2 and ocean dimethyl sulfide (DMS) emissions (e.g. Andres and Kasgnoc, 1998; Andreae and Crutzen, 1997). Sulfate particles strongly scatter incoming shortwave (SW) radiation, which helps to increase the planetary albedo and cool the surface. They also act as cloud condensation nuclei, leading to additional cloud droplets forming in supersaturated conditions, which increases cloud albedo and again cools the Earth system.

Atmos. Chem. Phys. Discuss., doi:10.5194/acp-2015-1017, 2016
Manuscript under review for journal Atmos. Chem. Phys.
Published: 18 January 2016

Historically, cooling from sulfate aerosol, predominantly in the more industrialised northern hemisphere, has been implicated by a range of modelling studies in disrupting climate since the mid-20th century. For instance Booth et al. (2012), Hwang et al. (2013), and Wilcox et al. (2013) discussed the importance of historical aerosol cooling in modulating large-scale temperature and precipitation patterns, while other studies such as Bollasina et al. (2011), Dong et al. (2014), and Polson et al. (2014) have looked at the impact of historical aerosols on regional climate features such as the monsoon systems or Sahelian rainfall.

The few studies that have investigated specific regional aerosol forcings (e.g. Shindell and Faluvegi (2009); Shindell et al. (2012); Teng et al. (2012)) typically used a single climate model at a time to investigate the climate response to idealised, historical, or projected forcings. However models vary considerably in their representation of aerosols and their radiative properties, resulting in a large uncertainty in aerosol radiative forcing (e.g. Myhre et al., 2013b; Shindell et al., 2013a). When investigating the climate response to regional aerosol emissions, such uncertainties are likely to be confounded even further by the variability between models in regional climate and circulation patterns, and variation in the global and regional climate sensitivity (the amount of simulated warming per unit radiative forcing). To best interpret the findings of single-model experiments with regional aerosol forcings, it is therefore critical to understand the range of uncertainty in the climate response that may arise as a result of structural and parametric differences between climate models.

We investigate here the range of variability that can arise in the translation of a regional emission perturbation to a climate (temperature) response, between three different state-of-the-art global climate models. We select as a case study the removal of SO_2 anthropogenic emissions from the region of China. Since China is currently the largest anthropogenic source region of sulfur dioxide (Smith et al., 2011) and hence anthropogenic aerosol, this regional perturbation represents a substantial modification to global aerosol levels, with the additional characteristic of being localised over a particular part of the world. This aspect of our experiment is distinct from many previous model intercomparison studies, which have typically compared the climate response in models forced by global historical trends in aerosols (for example, Shindell et al., 2015; Wilcox et al., 2013), or which have only considered the impact of regional emissions on long-range pollution transport and on radiative forcing (for example the HTAP and AeroCom experiments (HTAP, 2010; Yu et al., 2013; Kinne et al., 2006; Schulz et al., 2006; Textor et al., 2006)), but have not investigated the

Atmos. Chem. Phys. Discuss., doi:10.5194/acp-2015-1017, 2016
Manuscript under review for journal Atmos. Chem. Phys.
Published: 18 January 2016

range of model climate responses to a regionally localised emission perturbation. The potential importance of remote climate effects due to the strong zonal asymmetry created by such regional emissions has therefore not yet been explored in multi-model studies. Single-model studies such as Teng et al. (2012) suggest though that regionally localised forcings can produce significant climate teleconnections in at least the longitudinal direction.

In the following sections we first describe the three models employed, and our experimental setup (Sect. 2). We then present the results of the radiative flux and surface temperature responses to the removal of Chinese SO_2 (Sect. 3), and analyse the possible reasons for differences between the model responses (Sect. 4). Finally, in Sect. 5 we present our conclusions.

2 Model descriptions and experimental set-up

The three models we employ are the Hadley Centre Global Environment Model 3 – Global Atmosphere 4.0 (HadGEM3-GA4), the Community Earth System Model 1 (CESM1), and the Goddard Institute for Space Studies ModelE2 (GISS-E2). To allow the climate system to freely respond, the models are all used in a fully coupled atmosphere-ocean configuration. These three models all feature explicit aerosol modelling, and include both direct and indirect radiative effects of aerosols. However the models all vary in the details of the parameterisations used, the dynamical cores, radiation and cloud schemes, model grids and horizontal and vertical resolutions, land surface and ocean components, etc. This lack of common structural features make these three models well suited to contrast against one another and probe the range of potential model uncertainty, as we do here.

2.1 Model descriptions

2.1.1 HadGEM3-GA4

For HadGEM3, we use the Global Atmosphere 4.0 version of the model in a standard climate configuration with a horizontal resolution of 1.875° longitude x 1.25° latitude in the atmosphere, with 85 vertical levels and the model top at 85km, dynamically resolving the stratosphere. The atmosphere is coupled to the JULES land surface model, which includes 4 soil layers and 5 plant functional types. Although in principle this can be run in a fully

Atmos. Chem. Phys. Discuss., doi:10.5194/acp-2015-1017, 2016
Manuscript under review for journal Atmos. Chem. Phys.
Published: 18 January 2016

interactive 'Earth-System' mode with dynamic vegetation and a carbon cycle, here we prescribe fixed vegetation and also prescribe globally-uniform observed mass-mixing ratios for CO_2, CH_4, and other long-lived greenhouse gases, taking their year-2000 values from the CMIP5 historical dataset. A zonally-uniform present-day ozone climatology is also prescribed in the radiation scheme, derived from the SPARC dataset (Cionni et al., 2011). More detailed description and evaluation of the atmosphere and land-surface schemes can be found in Walters et al. (2014). The atmospheric model is also coupled to the NEMO dynamical ocean model (Madec, 2008) and CICE sea-ice model (Hunke and Lipscombe, 2008), which are run with a 1° horizontal resolution, and 75 vertical depth levels for the ocean.

Critical to our study is the representation of aerosols; we use the CLASSIC aerosol scheme, which is described and evaluated in Bellouin et al. (2011). CLASSIC is a mass-based scheme which includes an interactive representation of sulfate in three modes (Aitken, accumulation, and in-cloud), fossil-fuel black carbon, fossil-fuel organic carbon, and biomass-burning aerosol in three modes (fresh, aged, and in-cloud), dust in six size bins, and sea-salt in two modes (jet and film), as well as an offline biogenic aerosol climatology. The scheme can also include a representation of nitrate aerosol, but this option was not used here.

The sulfate component of the scheme (Jones et al., 2001) includes tracers for two gas-phase precursors: SO_2 from anthropogenic and natural sources, and DMS from natural sources. These are emitted into the atmosphere and can undergo advection, wet and dry deposition, or oxidation using prescribed 4D oxidant fields (Derwent et al., 2003). In CLASSIC, oxidation of SO_2 to SO_4 aerosol can proceed through three possible reaction pathways: in the gas phase by reaction with OH, or in the aqueous phase by reaction with either H_2O_2 or O_3.

The remaining aerosol species are emitted directly in the particulate phase, and all aerosol species can then undergo advection, wet and dry deposition, and interaction with radiation. The hygroscopic aerosols (sulfate, organic carbon, biomass-burning aerosol, sea-salt) can also interact with clouds via their role as cloud condensation nuclei. Cloud droplet number concentration and effective radius are determined from the concentration of these aerosols, which affects the simulated cloud lifetime (2^{nd} indirect effect) and cloud brightness (1^{st} indirect effect) as described in Bellouin et al. (2011) and Jones et al. (2001).

Atmos. Chem. Phys. Discuss., doi:10.5194/acp-2015-1017, 2016
Manuscript under review for journal Atmos. Chem. Phys.
Published: 18 January 2016

2.1.2 CESM1

CESM1 is run in its standard CAM5-Chem configuration (Tilmes et al., 2015) with a horizontal resolution of 2.5° longitude x 1.875° latitude, and 30 vertical levels, with the model top at approximately 40 km. The atmosphere is coupled to the Community Land Atmosphere version 4 land surface model (Lawrence et al., 2011). In the present configuration, the vegetation distribution is fixed at its 2005 distribution and the CO_2 concentration is specified. The atmosphere model is coupled to the POP2 ocean and CICE4 sea-ice models, with an equivalent resolution of 1°.

In the present CAM5-Chem configuration (Tilmes et al., 2015), we use a representation of tropospheric and stratospheric chemistry so that no chemical constituents are specified, other than specifying the long-lived greenhouse gases' concentrations in the surface layer. The gas-phase chemistry is coupled to the modal aerosol scheme MAM3 (Liu et al., 2012), so that the rate of formation of sulfate aerosols is dependent on the chemical state of the atmosphere. SO_2 from anthropogenic and natural sources can be converted to SO_4 through three oxidation pathways: by OH in the gas phase, or by either H_2O_2 or O_3 in the aqueous phase. In addition, the surface area of the prognostic tropospheric aerosols is used to compute heterogeneous reaction rates that affect gas-phase chemistry. Aerosols interact with climate through radiation and cloud-aerosol interactions.

2.1.3 GISS-E2

GISS-E2 is run in the configuration used for CMIP5 with a horizontal resolution of 2.5° longitude x 2° latitude, and 40 vertical levels, with the model top at 0.1 hPa (80 km). The atmospheric model is coupled to the dynamic Russell ocean model with horizontal resolution of 1° latitude x 1.25° longitude, and 32 vertical levels as described in Schmidt et al. (2013) and Russell et al. (1995).

Well-mixed greenhouse gases are prescribed as described in Miller et al. (2013), but methane is only prescribed at the surface and is otherwise interactive with the chemistry. The ozone distribution is prognostic throughout the simulated atmosphere, and the chemical mechanism is described in Shindell et al. (2013b). In general, other atmospheric gas and aerosol constituents are also simulated online and interact with each other (via oxidants in both the gas and aqueous phases, heterogeneous chemistry, aerosol-influenced gas photolysis, and

Atmos. Chem. Phys. Discuss., doi:10.5194/acp-2015-1017, 2016
Manuscript under review for journal Atmos. Chem. Phys.
Published: 18 January 2016

aerosol-coating of dust) and with climate (via radiative effects of ozone and methane, water vapour change due to chemistry, and aerosol direct and indirect effects) in a manner consistent with the physics of the rest of the GCM as described in Sect. 3b of Schmidt et al. (2013). For the sulfur scheme in particular, SO_2 from anthropogenic and natural sources can be oxidised to SO_4 aerosol through two reaction pathways: by OH in the gas phase, or by H_2O_2 in the aqueous phase.

Other aerosols include nitrate, elemental and organic carbon (Koch et al. 2011; 2006) along with secondary organic aerosols and natural sea-salt and mineral dust. Aerosol indirect effects are calculated as described in Menon et al. (2010).

2.2 Experimental setup

For this study we investigate the surface temperature response to an idealised regional emission perturbation, on a centennial timescale. Each model has a control simulation which is forced with the same anthropogenic emissions of aerosols and their precursors following the year-2000 ACCMIP emission inventory (Lamarque et al., 2010). The control simulations are run for 200 years with continuous year-2000 conditions. For each model, we then run a 200-year perturbation simulation in which SO_2 emissions from energy production, industry, transport, domestic use, and waste, are set to zero over the region of China, defined here to be the rectangular domain 80°-120°E, 20°-50°N. These emission sectors contribute 98.7% of the anthropogenic SO_2 emitted from this region, so this corresponds to a near complete removal of SO_2 emissions from this highly polluting area of the globe. Quantitatively, this perturbation reduces global anthropogenic SO_2 emissions from around 104 Tg yr^{-1} to 86 Tg yr^{-1}, a reduction of around 17 Tg yr^{-1}, or 16.5%.

3 Radiative forcing and climate response

We investigate the change in the mean state of the models by taking averages over the last 150 years of the 200-year-long simulations (the first 50 years were discarded as spin-up), and taking the difference between the perturbation simulation and the control simulation. As well as plotting maps of 2D variables, we also calculate area-weighted means of temperature, short-wave radiative flux, and aerosol optical depth, both globally and for an east China

Atmos. Chem. Phys. Discuss., doi:10.5194/acp-2015-1017, 2016
Manuscript under review for journal Atmos. Chem. Phys.
Published: 18 January 2016

region (E. China) defined as 100°-120°E, 20°-40°N. This region is found to contain the most intense changes in sulfate aerosol in all three models, and is used from here on to quantify the magnitude of local changes over China. The global- and regionally-averaged quantities are tabulated in Table 1, along with the total sulfate burdens over the globe and E. China, and the ratios of AOD to sulfate burden and SW flux to AOD changes.

The anticipated immediate consequence of removing SO_2 emissions from China is that there will be a reduction in the amount of sulfate aerosol formed, leading to a positive shortwave (SW) radiative forcing. Figure 1 shows the changes in net downward top-of-atmosphere (TOA) SW radiative flux in each of the three models. For HadGEM3-GA4 and GISS-E2, the plot is stippled in locations where the change exceeds two standard deviations, estimated for HadGEM3-GA4 from the grid-point standard deviations from six year-2000 control runs with perturbed atmospheric initial conditions, and for GISS-E2 from 12 non-overlapping 150-year sections of a 1900-year-long pre-industrial control simulation that had reached radiative equilibrium.

Figure 1 reveals that there is a very substantial variation between the models in the intensity of the local radiative flux change over China. GISS-E2 shows a fairly weak increase in net downward SW flux over E. China, with a local increase (from Table 1) of 0.91 W m^{-2} and an insignificant global mean change (-0.034 W m^{-2}), whereas HadGEM3-GA4 shows a very pronounced change of 5.3 W m^{-2} locally over E. China, and a global mean value of 0.28 W m^{-2}. CESM1 lies in the middle, with a moderate local SW flux change of 4.2 W m^{-2}, and 0.19 W m^{-2} in the global mean. Between GISS-E2 and HadGEM3-GA4, there is a 6-fold increase in the intensity of the local radiative flux change over E. China.

Because these are fully coupled simulations, the change in the TOA SW flux does not provide a measure of the shortwave radiative forcing, since the underlying climate has been allowed to adjust, potentially allowing feedbacks on clouds, and snow and ice cover. A complementary pair of atmosphere-only simulations, where sea-surface temperatures (SSTs) and sea-ice cover were prescribed to year-2000 values, were run with HadGEM3-GA4 to diagnose the effective radiative forcing (ERF) – the change in TOA radiative flux when feedbacks due to the slow response of the ocean are prevented (Andrews et al., 2010). The global SW ERF due to removing SO2 from China in these fixed-SST simulations is 0.18 W m^{-2}, 35% smaller than the 0.28 W m^{-2} change in the fully coupled case. However, locally over the E. China region, the fixed-SST change was found to be 4.2 W m^{-2}, which is only 21% lower than the 5.3 W m^{-2}

Atmos. Chem. Phys. Discuss., doi:10.5194/acp-2015-1017, 2016
Manuscript under review for journal Atmos. Chem. Phys.
Published: 18 January 2016

value in the fully coupled experiment. Moreover, the spatial map of the SW flux anomaly over China is very similar between the two experiments (Supplementary fig. S1). At least in HadGEM3-GA4, over E. China the change in sulfate therefore appears to be the dominant driver of the change in TOA SW flux, and the local change in SW flux over this region is reasonably representative of the local radiative effect of the sulfate perturbation even in the fully-coupled simulations with this model. The same is less true of the global-mean values because of positive feedback from ice melt in the Arctic, and also some small but widespread changes in cloud cover, which globally add up to a sizeable effect in the coupled simulations (not shown).

Based on the fully coupled simulations, the substantial differences in the intensity of SW flux changes over China ultimately translate to very pronounced differences in the strength of the resulting climate response. Figure 2 shows the change in surface air temperatures between the perturbation and control runs for each of the three models. Again stippling indicates the response exceeds the 2σ level in HadGEM3-GA4 and GISS-E2. The difference between GISS-E2 and HadGEM3-GA4 is particularly striking. Apart from a small warming in parts of eastern China by around 0.1 K, there is virtually no coherent temperature response across the rest of the globe in GISS-E2. The global mean temperature change (Table 1) is -0.028 K and is not significant. In contrast HadGEM3-GA4 displays significant warming across almost all of the northern hemisphere, with much larger increases in temperature between 0.4-1 K in many regions, not only in China but also in much of the US, northern Eurasia, and the Arctic. The global mean temperature response is +0.11 K. CESM1 sits again in the middle, with clear warming responses between 0.2-0.5 K over much of eastern Europe, Asia, and the west Pacific. Overall the warming response is still less strong and less widespread than in HadGEM3-GA4, with a global mean warming of +0.054 K.

The spatial pattern of warming over Europe and Asia in CESM1 bears some qualitative similarity though to the pattern over the same region in HadGEM3-GA4, suggesting that there may be a similar mode of global response to heating over eastern China in these models, at least across the Eurasian continent. The dynamical mechanisms through which local aerosol emissions are translated to remote response are beyond the scope of this manuscript though. Whether GISS-E2 would have displayed the same pattern had the radiative forcing over China been stronger is impossible to tell from these results; given the small magnitude of the SW flux change it seems that most of the spatial pattern in the temperature response in GISS-

Atmos. Chem. Phys. Discuss., doi:10.5194/acp-2015-1017, 2016
Manuscript under review for journal Atmos. Chem. Phys.
Published: 18 January 2016

E2 can be attributed to internal variability – the largest changes in temperature seen in this model are in fact a region of cooling over the north-west Atlantic, which is mostly not significant and appears instead to be the result of particularly large internal variability in this region.

4 Exploring drivers of diversity

We investigate the differences between these models that lead to such a large variation in the predicted temperature response. We explore below a number of possible sources of discrepancy.

4.1 Differences in simulated aerosol amounts

We address first the possibility that differences in the aerosol schemes themselves, lead directly to very different aerosol loadings between the models, despite the identical change in SO_2 emissions applied. Figure 3 shows the change in column-integrated SO_4 in each model as a result of removing Chinese SO_2 emissions. The models vary in both the distribution and magnitude of SO_4 reductions. In particular, HadGEM3-GA4 has the reduction in SO_4 burden fairly concentrated over China. CESM1 and GISS-E2 simulate more diffuse changes in SO_4 which extend further downwind from the source region, giving a larger spatial footprint. This difference in spatial extent of the SO_4 field from Chinese SO_2 seems to be due to particularly fast conversion of SO_2 to SO_4 in HadGEM3-GA4 resulting in much more concentrated changes in SO_4 close to the source. For GISS-E2 and HadGEM3-GA4 where more detailed diagnostics were available, we find that the SO_2 lifetime is around 1.8 times shorter in HadGEM3-GA4, associated with around 45% higher wet oxidation rates in this model. This difference is due in part to the inclusion of an additional wet oxidation pathway in HadGEM3-GA4: whereas GISS-E2 only includes wet oxidation of SO_2 by H_2O_2 (around 730 kg(S) s^{-1} globally integrated), HadGEM3-GA4 includes wet oxidation by both H_2O_2 and O_3, each of which contribute similarly in this model (around 540 kg(S) s^{-1} and 520 kg(S) s^{-1} respectively).

Globally integrated, HadGEM3-GA4 and GISS-E2 simulate fairly similar reductions in SO_4 burden, at -0.070 Tg and -0.077 Tg respectively (Table 1). This, combined with the more

Atmos. Chem. Phys. Discuss., doi:10.5194/acp-2015-1017, 2016
Manuscript under review for journal Atmos. Chem. Phys.
Published: 18 January 2016

Atmospheric Chemistry and Physics Discussions

spread-out SO_4 field in GISS-E2, means that locally over eastern China HadGEM3-GA4 has a much more intense reduction in SO_4 burden, with 50% of the global reduction occurring over E. China in HadGEM3-GA4 (-0.035 Tg), compared with only 21% (-0.016 Tg) in GISS-E2. CESM1, by contrast, simulates almost double the global change in SO_4 burden as the other two models, with -0.136 Tg. This means that although the SO_4 reduction spreads further from the source in CESM1 than in HadGEM3-GA4, CESM1 still has a similar reduction to HadGEM3-GA4 locally over E. China (-0.039 Tg).

Given that HadGEM3-GA4 and GISS-E2 simulate a similar global reduction in SO_4, it is surprising that there is such a difference in the magnitude of their climate responses. Also, given that CESM1 simulates a much larger global reduction in SO_4 than the other two models, it is similarly surprising that this model does not have the largest response. A partial explanation may be found by inspecting the change in total aerosol optical depth (AOD), which is a more direct measure of the radiative properties of the aerosol column. Unfortunately, the AOD diagnosed by the models is not completely equivalent: HadGEM3-GA4 diagnosed clear-sky AOD, which is done in this model by calculating the relative humidity in the cloud-free portion of each grid-box, and using this adjusted humidity to calculate the size of the aerosol droplets in the optical depth calculation (Bellouin et al., 2007). However CESM1 uses the unadjusted grid-box relative humidity to calculate the droplet sizes in its optical depth calculation, thereby providing an all-sky AOD calculation (Neale et al., 2012). GISS-E2 diagnosed both all-sky and clear-sky AOD, and unless otherwise stated we compare here its clear-sky AOD, as it is more directly comparable with satellite retrievals of AOD (Kahn et al., 2010; Levy et al., 2013). Figure 4 shows these changes in AOD at the 550nm wavelength for the three models.

As with the radiative flux change, there is a large range in the magnitude of local AOD reduction, with E. China AOD reductions ranging from 0.047 in GISS-E2 to 0.287 in HadGEM3-GA4, i.e. about 6 times higher (Table 1). This is comparable to the approximately 6-fold range of SW flux change found over this region. Globally averaged, HadGEM3-GA4 also has a much larger AOD reduction than GISS-E2; 0.0042 compared with an almost negligible 0.0003 in GISS-E2, despite these two models having a similar change in global SO_4 burden. The much lower globally-averaged value in GISS is partly due to a very small but quite zonally-uniform compensating increase in nitrate aerosol, (absent in HadGEM3-GA4), which occurs across the northern hemisphere (not shown). However, the global

Atmos. Chem. Phys. Discuss., doi:10.5194/acp-2015-1017, 2016
Manuscript under review for journal Atmos. Chem. Phys.
Published: 18 January 2016

change in sulfate-only optical depth in GISS-E2 is still only half that in HadGEM3-GA4 (not shown), and locally around eastern China we find the increase in nitrate optical depth in GISS-E2 is at least an order of magnitude smaller than the decrease in sulfate optical depth, and so nitrate compensation does not substantially contribute to the discrepancy in local AOD changes. We therefore still find that HadGEM3-GA4 simulates a considerably larger change in sulfate optical depth per unit change in SO_4 burden at both global and local scales. Having the largest change in AOD per unit change in aerosol burden (Table 1) appears to be key to this model simulating the largest climate response.

Comparing the clear-sky and all-sky AOD for GISS-E2 (for which we have both diagnostics), we find that the simulated reduction in all-sky AOD (-0.183) is much larger than the reduction in clear-sky AOD (-0.047). We cannot be sure that the same would apply to CESM1, but it suggests that we might expect the all-sky values we have for CESM1 to be larger than the equivalent clear-sky values. Given this, it is surprising to find reductions of all-sky AOD in CESM1 for the E. China region of -0.076 and for the global mean of -0.0013 (Table 1), which lie in between the clear-sky values of GISS-E2 and HadGEM3-GA4 even though CESM1 had the largest change in SO_4 burden both locally and globally.

The change in SW radiative flux and the final climate response seem to correlate with the change in AOD much better than with the change in SO_4 burden for HadGEM3-GA4 and GISS-E2, where over China there is a 6-fold difference both in AOD and in SW flux change between these two models. For CESM1, the all-sky AOD changes over E. China are about 1.6 times larger than the clear-sky changes in GISS-E2 (Table 1). If we used instead all-sky AOD from GISS-E2 (not shown in Table 1), we find that the AOD change over E. China is more than 2 times smaller in CESM1 than in GISS-E2. However, the change in TOA SW over the same region is about 4.7 times larger in CESM1, and so it seems that unlike the discrepancies between HadGEM3-GA4 and GISS-E2, differences in the AOD response cannot explain the difference in the magnitudes of radiative flux change between CESM1 and GISS-E2 (see Sect. 4.3).

4.1.1 Validation of aerosol fields

To get an indication of whether the model-simulated AODs are realistic in the region of interest, we compare the mean AOD from each model's control run with station observations

Atmos. Chem. Phys. Discuss., doi:10.5194/acp-2015-1017, 2016
Manuscript under review for journal Atmos. Chem. Phys.
Published: 18 January 2016

in Asia from the AERONET radiometer network (Holben et al., 2001). Because of the limited number of stations in the region with long data records, we use the observed AOD at 500 nm from all AERONET stations able to provide an annual mean estimate for at least one year, averaged over all years for which an annual mean was available, (generally ranging between 1998 and 2014 in different stations), and compare this with the annual mean AODs at 550 nm from the three models, masked to the locations of the AERONET stations (Supplementary fig. S2). Focusing on stations in E. China (eight in total), we find that HadGEM3-GA4 compares best with AERONET in this region with a mean station bias of -22%, whilst both GISS-E2 and CESM1 appear to be biased lower in this part of the world, with mean biases of -56% and -60% respectively.

We also calculate the area-weighted mean AOD as observed by the MODIS and MISR satellite instruments. The MODIS (Moderate Resolution Imaging Spectroradiometer) instrument is flown on both the Terra and Aqua satellites, whilst MISR (Multi-angle Imaging SpectroRadiometer) is flown on Terra. For MODIS we use the collection 6 combined Deep Blue + Dark Target monthly AOD product at 550 nm (Levy et al., 2013) (available from https://ladsweb.nascom.nasa.gov/), averaged from both Terra and Aqua satellites, and take a 10-year average from 2003-2012 (2003 being the earliest year that data from both satellites is available). For MISR we use the best estimate monthly AOD product (Kahn et al., 2010) version 31 (available from https://eosweb.larc.nasa.gov/) at 550 nm over a 15-year averaging period, from 2000-2014 (2000 being the earliest year MISR data is available). For MODIS the area-weighted E. China mean AOD is 0.51, whilst for MISR it is 0.31, so regionally there is a considerable uncertainty in these observations. HadGEM3-GA4 overestimates the AOD compared with both instruments, with a regional average AOD of 0.58, whilst GISS-E2 and CESM1 underestimate with regionally-averaged AODs of 0.23 for both models. Globally the two instruments are in better agreement, with MODIS giving a global average AOD of 0.17 and MISR giving 0.15. Again HadGEM3-GA4 overestimates global AOD compared with both instruments (0.22) whilst GISS-E2 and CESM1 both underestimate (0.13 and 0.12). Given that CESM1 diagnosed all-sky AOD, whereas satellite retrievals are only possible for clear-sky conditions, the underestimate for this model is likely greater than these numbers suggest.

There is considerable variation in the observations as well as the models. Globally GISS-E2 seems to compare best against MODIS and MISR, though tentatively HadGEM3-GA4 seems

Atmos. Chem. Phys. Discuss., doi:10.5194/acp-2015-1017, 2016
Manuscript under review for journal Atmos. Chem. Phys.
Published: 18 January 2016

to have the more accurate AOD over China, comparing best regionally with both AERONET and MODIS, though poorer against MISR. This suggests that the more concentred sulfate aerosol burden and larger AOD reduction simulated by HadGEM3-GA4 over this region may be more realistic. However we note though that since these observations only measure total AOD and cannot differentiate by species, the comparison cannot show for certain that the higher sulfate optical depth specifically is more realistic in HadGEM3-GA4. The AOD reduction over E. China due to removing Chinese SO_2 represents 50% of the climatological total AOD in HadGEM3-GA4 over the region, compared with 34% in CESM1 and only 20% in GISS-E2. Even if the total AOD in HadGEM3-GA4 is more realistic, there is still considerable variation between the models as to what fraction of that total AOD is due to Chinese SO_2 emissions.

For HadGEM3-GA4 and GISS-E2, for which sulfate mixing-ratio diagnostics were available for individual model levels, we therefore also compared against the surface sulfate observations conducted in China reported by Zhang et al. (2012) for 2006-2007 (Supplementary fig. S3). However, both models performed extremely poorly, with HadGEM3-GA4 having a mean bias of -71% (-66% if urban stations are excluded), and GISS-E2 having a mean bias of -87% (-86% when urban stations are excluded). Although HadGEM3-GA4 is closer to the observed value, the large underestimation despite the relatively good column AOD comparison suggests that the model has difficulty representing the vertical profile of sulfate aerosol, and so this comparison with surface measurements may not be that useful in constraining the sulfate optical depth or column-integrated burdens. Large underestimations of surface sulfate concentration over East Asia have been reported previously for two other models, MIROC and NICAM, by Goto et al. (2015), suggesting that this is a problem common to many current generation models.

It seems plausible that any differences in the processing of sulfate aerosol would apply to all polluted regions, and not just over China. Indeed, the spatial pattern of the climatological sulfate burden over other major emission regions like the United States shows a similar characteristic to that over China, with HadGEM3-GA4 having a higher burden close to the emission source regions, whilst GISS-E2 has a more diffuse sulfate distribution (Supplementary fig. S4). With this in mind we also validated these two models against surface sulfate observations from the Interagency Monitoring of Protected Visual Environments (IMPROVE) network in the United States (Malm et al., 1994), a dataset with a

Atmos. Chem. Phys. Discuss., doi:10.5194/acp-2015-1017, 2016
Manuscript under review for journal Atmos. Chem. Phys.
Published: 18 January 2016

far more extensive record than the Zhang et al. (2012) dataset for China. Taking 61 IMPROVE stations which have data for at least 6 years between 1995 and 2005, we find that over the United States both models are biased slightly high, with GISS-E2 performing relatively better with a mean bias of +10.1%, but HadGEM3-GA4 somewhat worse with +44.5%. However, we find that the larger mean bias in HadGEM3-GA4 comes mainly from an incorrect spatial distribution (Supplementary fig. S5), with a high bias on the West Coast but a pronounced low bias in surface SO_4 on the East Coast. Consequently, this comparison would suggest that HadGEM3-GA4 in fact has too little sulfate around the principal US emission regions on the East Coast, even though over that area HadGEM3-GA4 actually has a larger column-integrated sulfate burden (Supplementary fig. S4) and a larger AOD (not shown) than GISS-E2, as was the case for China.

Validation with surface observations therefore seems insufficient to constrain which model performs better with regard to the more climate-relevant column-integrated quantities of sulfate burden and AOD. Returning to Asia, we therefore also tried validating HadGEM3-GA4 and GISS-E2 using sulfate wet deposition observations, which should be less sensitive to the precise vertical profile of sulfate in the models. We use the 3-year mean wet deposition data from 2000-2002 described in Vet et al. (2014) and provided by the World Data Centre for Precipitation Chemistry (http://wdcpc.org, 2014), taking the 6 stations located in China. We exclude the station in Guizhou province in southern China where HadGEM3-GA4 has a bias of +590% and GISS-E2 a bias of +253%. This station only provided data for one year and was flagged as having a high uncertainty in the Vet et al. (2014) dataset; it is also located in a mountainous region and so it could equally be that the models cannot resolve the specific local conditions. Removing this station from the analysis we find for the remaining 5 stations in China that HadGEM3-GA4 performs well with a mean bias of -3.9%, compared with -64.8% for GISS-E2. This gives an indication that HadGEM3-GA4 has more realistic sulfate deposition directly over China, though the sample size is very small. If we broaden the analysis to include all stations described as being broadly in Asia – an additional 32 stations – then the mean bias for HadGEM3-GA4 is worsened (-41.8%), whilst the bias in GISS-E2 is slightly improved (-54.1%). HadGEM3-GA4 still performs better over the Asian region as a whole, though less dramatically so (Supplementary fig. S6).

4.2 Differences in cloud effects

Atmos. Chem. Phys. Discuss., doi:10.5194/acp-2015-1017, 2016
Manuscript under review for journal Atmos. Chem. Phys.
Published: 18 January 2016

Sulfate aerosol exerts indirect radiative effects by modifying cloud properties. The strength of these indirect effects is highly uncertain (e.g. Boucher et al., 2013) and differs substantially between the models, having been shown to contribute substantially to inter-model variation in historical aerosol forcing (Wilcox et al., 2015). Differences in the underlying climatologies of the models, particularly with regard to cloud distributions, could also be important since the radiative effect of sulfate aerosol is modulated by the reflectivity of the underlying surface in the radiation scheme (Chýlek and Coakley, 1974; Chand et al., 2009), which may often be a cloud-top.

In our case, the good correspondence between higher (clear-sky) AOD change in HadGEM3-GA4 and higher (all-sky) SW flux change in this model would suggest that the cloud effects are not the root cause of the larger radiative response in this model.

Additionally clear-sky SW flux diagnostics were available for HadGEM3-GA4 and GISS-E2 (Supplementary fig. S7), and comparing them with the all-sky SW flux anomalies we still find a large - albeit smaller (3-fold rather than 6-fold) - discrepancy between these two models. This reduced difference between GISS-E2 and HadGEM3-GA4 in the clear-sky compared with all-sky anomaly is hard to apportion, because the all-sky response incorporates both aerosol indirect effects and also dynamical feedbacks on clouds. In fact, in both models the clear-sky SW change turns out to be larger than the all-sky SW change, which is opposite to what we would expect from a simple amplification of the radiative response due to indirect effects. In particular GISS-E2 simulates an increase in cloudiness in East China when sulfate is removed (not shown), which partially offsets the direct forcing of reduced SO_4 and results in a smaller all-sky flux change than clear-sky flux change (0.91 Wm^{-2} compared with 1.8 Wm^{-2}). HadGEM3-GA4 has mixed changes in cloud amount over East Asia (not shown) and has a smaller difference between all-sky and clear-sky flux changes (5.3 Wm^{-2} and 5.8 Wm^{-2} respectively), explaining why there is a bigger discrepancy between these two models in the all-sky forcing. Nonetheless, the fact that there is still a 3-fold difference in clear-sky flux indicates that even in a cloud-free world, there would be large disagreement in the models' SW forcing over China, and so cloud responses are not the primary driver of the discrepancies, although cloud feedbacks are clearly important in modulating the final magnitude of the discrepancy.

Diagnostics for clear-sky radiative fluxes and cloud amount were not available for CESM1, so we are unable to make a similar comparison for this model.

Atmos. Chem. Phys. Discuss., doi:10.5194/acp-2015-1017, 2016
Manuscript under review for journal Atmos. Chem. Phys.
Published: 18 January 2016

Atmospheric Chemistry and Physics Discussions

4.3 Differences in aerosol forcing efficiency

An additional source of discrepancy between the models lies in differences in the aerosol radiative forcing efficiency – the forcing that results from a given aerosol optical depth or burden (e.g. Samset et al, 2013). A previous model intercomparison looking at radiative forcing as part of the AeroCom Phase II study found that there was a large variation in the radiative forcing due to aerosol-radiation interactions per unit AOD between different participating models (Myhre et al., 2013a) on a global scale.

Globally-averaged, the changes in radiative flux and AOD are too small in our experiments to calculate an accurate ratio, but instead we calculate here a regional radiative efficiency for HadGEM3-GA4 and GISS-E2 by taking the change in clear-sky SW flux over the 100-120E, 20-40N region (Sect. 4.2), and dividing by the clear-sky AOD change over the same region (Table 1). This is not directly comparable with previous studies like Myhre et al. (2013a), as we use a regionally-averaged number instead of globally-averaged, and for the numerator we use the change in clear-sky SW flux rather than the clear-sky radiative forcing. Consequently we use this metric here mainly to qualitatively highlight differences between the models.

As noted in Sect. 4.1 and 4.2, over the eastern China region HadGEM3-GA4 has a 6-fold larger mean AOD reduction (-0.29) compared with GISS-E2 (-0.047), but only a 3-fold larger clear-sky SW change (5.8 W m^{-2} compared with 1.8 W m^{-2}). As a result the regional radiative efficiency for HadGEM3-GA4 is only about half that of GISS-E2 (-20.3 W m^{-2} compared with -39.1 W m^{-2}). If we normalise by the change in sulfate burden instead of the AOD integrated over the same region, however, we find the opposite relationship: HadGEM3-GA4 has a larger regional mean change in clear-sky SW flux per Tg sulfate than GISS-E2 (-167.1 W m^{-2} Tg^{-1} compared with -117.7 W m^{-2} Tg^{-1}). The much larger AOD per unit mass of sulfate simulated in HadGEM3-GA4 therefore outweighs the smaller radiative response per unit AOD. Curiously Myhre et al. (2013a) reported results that were qualitatively the inverse of what we show here, finding that the atmospheric component of GISS ModelE2 has a smaller sulfate radiative forcing than that of HadGEM2 (HadGEM3's predecessor, with a very similar aerosol scheme) when normalised by AOD, but larger when normalised by column-integrated sulfate burden. The reason for the discrepancy is not clear, though the aforementioned fact that we calculate our numbers for a specific region means that there may

Atmos. Chem. Phys. Discuss., doi:10.5194/acp-2015-1017, 2016
Manuscript under review for journal Atmos. Chem. Phys.
Published: 18 January 2016

be important local factors. For instance, the forcing per unit AOD will be influenced by the vertical distribution of the aerosol (Myhre et al., 2013a), which could vary between models in different parts of the world.

Making an equivalent comparison for CESM1 is hindered by the lack of clear-sky diagnostics available from this model for these simulations. What we can note is that if we instead use the all-sky change in SW flux over East China, normalising by AOD we find a much larger SW change per unit AOD in CESM1 than in HadGEM3-GA4 or GISS-E2 (-55.0 W m^{-2} compared with -18.6 W m^{-2} and -19.6 W m^{-2}) (Table 1). Normalising by all-sky AOD in GISS-E2 (which provides both clear-sky and all-sky diagnostics) however gives a comparatively even smaller value (-4.95 W m^{-2}). Normalised by the change in regional sulfate burden instead, CESM1 sits in the middle with -107.7 W m^{-2} Tg^{-1}, compared with HadGEM3-GA4's -153.5 W m^{-2} Tg^{-1} (quite close to its clear-sky normalised value), and GISS-E2's -56.6 W m^{-2} Tg^{-1} (much smaller than its clear-sky normalised value). These results suggest that either CESM1 has a large radiative efficiency per unit AOD which compensates for its much smaller AOD per mass of sulfate, or else there are large cloud responses – either due to a particularly strong aerosol indirect effect, or a dynamical reduction in local cloudiness – which considerably amplify the radiative effect of a relatively small AOD reduction in this model.

The Myhre et al. (2013a) AeroCom intercomparison found that globally, the atmospheric component of CESM1 (CAM5.1) did indeed have a much higher sulfate radiative efficiency than the atmosphere-only version of GISS-E2. In their case, they found CAM5.1 to have approximately 2.25 times higher direct radiative forcing per unit AOD than GISS-E2. However, the study also found that, globally, the atmospheric component of HadGEM2 had a very similar forcing efficiency to CAM5.1. Given that our regional values from GISS-E2 and HadGEM3-GA4 conflict qualitatively with the global values from the AeroCom study though, this probably does not provide a strong indication of which factor is more likely the dominant driver of the relatively large response in CESM1 despite its modest AOD change.

4.4 Differences in climate sensitivity

So far we have discussed mainly factors which influence the translation of a change in aerosol precursor emissions to a radiative heating, and these varied strongly between the models.

Atmos. Chem. Phys. Discuss., doi:10.5194/acp-2015-1017, 2016
Manuscript under review for journal Atmos. Chem. Phys.
Published: 18 January 2016

Atmospheric Chemistry and Physics Discussions

There is a final step in arriving at the climate response, which is the translation of a given radiative heating into a surface temperature change. The climate sensitivity – the amount of warming simulated per unit radiative forcing – is also well known to vary considerably between models, globally (Flato et al., 2013) and regionally (Voulgarakis and Shindell, 2010), and this will additionally impact the strength of the final response. Climate sensitivity is typically estimated from a 2x or 4x global CO_2 simulation, giving a large response and a large forcing from which to calculate the ratio. For GISS-E2, a climate sensitivity value of 0.6 K $(W\ m^{-2})^{-1}$ was found in the IPCC AR5 report from a 4x CO_2 simulation (Flato et al., 2013) using the regression method of Gregory et al. (2004) to estimate radiative forcing. For CESM1, a value of 1.1 K $(W\ m^{-2})^{-1}$ is obtained from values from a 2x CO_2 simulation (Meehl et al., 2013), noting that in this case the radiative forcing was calculated using the stratospheric adjustment method (Hansen et al., 2005). For HadGEM3-GA4, we use a 100-year 2x CO_2 simulation that was performed separately as part of the Precipitation Driver Response Model Intercomparison Project (Samset et al., in preparation), which gives a value of 1.1 K $(W\ m^{-2})^{-1}$ based on the Gregory method.

While CESM1 and HadGEM3-GA4 both have very similar climate sensitivities, we see that GISS-E2 has a particularly small sensitivity – in fact, the smallest value of all the CMIP5 models reported in the AR5 report (Flato et al., 2013). This presumably compounds the fact that GISS-E2 simulates the smallest SW flux change of the three models, ensuring that the resulting surface temperature response is comparatively smaller still. Differences in climate sensitivity do not seem to explain any of the variation in the magnitude of the response between CESM1 and HadGEM3-GA4, at least based on these values. However, it is worth noting that the climate sensitivity values that we report are derived from global CO_2 forcings, whereas in our case we are looking at the translation of a very regional forcing into a global response. It is not trivial that the global-mean temperature response to a regionally localised forcing is a function only of the resulting globally-averaged forcing, and in particular it may be that different models are more or less sensitive to forcings in specific regions. Unfortunately we know of no study that has calculated climate sensitivity to regional forcings in single or multi-model frameworks. Shindell (2012) calculated regional climate sensitivities to forcings imposed in different latitudinal bands for the GISS-E2 model, finding that there is considerable regional variation relative to the global climate sensitivity. In that study, estimates of the response to regional forcings in 3 other global climate models, based on the GISS-E2 regional sensitivities, are found to largely agree to within +/- 20% with the full

Atmos. Chem. Phys. Discuss., doi:10.5194/acp-2015-1017, 2016
Manuscript under review for journal Atmos. Chem. Phys.
Published: 18 January 2016

simulations however, suggesting that regional sensitivities (relative to a model's global sensitivity) may not vary that much between models.

5 Conclusions

By applying an identical regional perturbation to anthropogenic SO_2 emissions in three different climate models, we observe three markedly different resulting climate responses, ranging from virtually no coherent surface air temperature response in one model (GISS-E2), to pronounced surface warming all across most of the northern hemisphere in another (HadGEM3-GA4). The third model (CESM1) sits in the middle in terms of both magnitude and spatial extent of the temperature response. This huge variation in climate response corresponds to a similarly large variation in the SW radiative flux change following the reduction in sulfate aerosol. All three models show a fairly localised increase in net downwards SW radiation over China as a result of reduced SO_2 emissions from this region, however the magnitude of this radiative heating is substantially greater in HadGEM3-GA4 than in CESM1, which is substantially greater still than in GISS-E2. The response in GISS-E2 is so weak that temperature changes are largely not detectable above the internal variability of the model. The stronger heating in CESM1 and HadGEM3-GA4 produces much more pronounced temperature changes, and even though the radiative heating is localised over China, the temperature responses in these two models are much more spread out, particularly in the zonal direction. This is consistent with the findings of Shindell et al. (2010), who found that the temperature response to inhomogeneous aerosol forcings is more uniform and extends much further from the forcing location in the zonal direction than in the meridional direction.

Comparing the models we find very different changes in the SO_4 mass change due to removing SO_2 emissions from China, very different ratios of AOD change per mass of sulfate, and different radiative flux changes per unit AOD. These differences are compounded further by variations in cloud responses, climate sensitivity, and the feedbacks on other aerosol species such as nitrate, which diversify the response further. In addition to differences in the total changes in sulfate and AOD, we find there are also substantial differences in the spatial distribution of the changes, attributed to differences in the rate of chemical conversion of SO_2 to SO_4 which influences how concentrated the aerosol changes are around the emission

Atmos. Chem. Phys. Discuss., doi:10.5194/acp-2015-1017, 2016
Manuscript under review for journal Atmos. Chem. Phys.
Published: 18 January 2016

region. This implies that even if both the AOD per sulfate burden and the forcing per unit AOD were identical among the three models, they would still have different distributions of radiative forcing.

Specifically, we find that CESM1 simulates the largest reduction in sulfate burden both globally and locally. HadGEM3-GA4 has the smallest reduction in sulfate burden globally and the second largest reduction regionally, yet it produces by far the largest reduction in AOD both globally and regionally over E. China. This much larger change in AOD per change in sulfate burden in HadGEM3-GA4 results in the largest radiative changes and the largest temperature response in this model. Though both GISS-E2 and CESM1 simulate much smaller changes in AOD than HadGEM3-GA4, still the SW flux changes and temperature responses produced are very different between these two models. In GISS-E2 the radiative effect of sulfate burden changes appears smallest, and this combines with compensating increases in local cloud amount over China and nitrate aerosol globally to reduce the radiative response yet further, and a smaller climate sensitivity results in this being translated into a largely negligible temperature response.

There are no direct observations of sulfate radiative forcing, nor of sulfate optical depth or vertically-integrated burden, and so we have tried validating the aerosol component of the models with a range of surface and satellite-based measurements of total aerosol optical depth, surface sulfate concentration, and sulfate wet deposition. All the models have biases, and no model performs best against all the observational datasets used. Tentatively HadGEM3-GA4 seems to perform best over China against observations of both total AOD and sulfate wet deposition, though over some other parts of the world this model performed slightly poorer, e.g. for global AOD and US surface sulfate concentrations. However, the main conclusion is that comparison against all existing observational measures is unable to satisfactorily constrain which model response is more realistic. The model with the largest sulfate mass change (CESM1) did not have the largest radiative or climate response, and two models with a similar AOD change (CESM1 and GISS-E2) had markedly different radiative and climate responses. Given the range of discrepancies that we find in all steps along the conversion of SO_2 change to SO_4 change to AOD change to radiative forcing to temperature response, it seems that knowing how accurate a model is with respect to either sulfate concentrations or total AOD is far from sufficient to determine whether the climate response to a regional aerosol perturbation is similarly accurate.

Atmos. Chem. Phys. Discuss., doi:10.5194/acp-2015-1017, 2016
Manuscript under review for journal Atmos. Chem. Phys.
Published: 18 January 2016

We have only looked here at surface temperature, which is a particularly direct measure of the climate response. The response of other, less well-constrained, climate variables such as precipitation might be expected to show even greater variation. Our results show that there remains a very large uncertainty in current climate models in the translation of aerosol precursor emissions into a climate response, and imply that care must be taken not to over-interpret the results of studies performed with single models.

On a more optimistic note, we remark that in the two models which showed the more substantial change in SW radiative flux (CESM1 and HadGEM3-GA4), both also show a remarkably strong remote temperature response to a relatively localised northern-midlatitude heat source, with qualitatively similar temperature change patterns that extend across much of the hemisphere, indicating that there may be some agreement on the response to a given regional forcing, if not on the forcing itself.

Data availability

Model output data from all simulations described here is available upon request from the corresponding author.

Acknowledgements

MK and AV are supported by the Natural Environment Research Council under grant number NE/K500872/1. Also, we wish to thank the European Commission's Marie Curie Actions International Research Staff Exchange Scheme (IRSES) for funding MK's placement at NASA GISS and Columbia University and facilitating interactions on this work with the US colleagues, as part of the Regional Climate-Air Quality Interactions (REQUA) project. Simulations with GISS-E2 used resources provided by the NASA High-End Computing (HEC) Program through the NASA Center for Climate Simulation (NCCS) at Goddard Space Flight Center. Simulations with HadGEM3-GA4 were performed using the MONSooN system, a collaborative facility supplied under the Joint Weather and Climate Research Programme, which is a strategic partnership between the Met Office and the Natural Environment Research Council. We specifically thank Dr. Fiona O'Connor, Dr. Jeremy

Atmos. Chem. Phys. Discuss., doi:10.5194/acp-2015-1017, 2016
Manuscript under review for journal Atmos. Chem. Phys.
Published: 18 January 2016

Walton, and Mr. Mohit Dalvi from the Met Office for their support with using the HadGEM3-GA4 model.

Atmos. Chem. Phys. Discuss., doi:10.5194/acp-2015-1017, 2016
Manuscript under review for journal Atmos. Chem. Phys.
Published: 18 January 2016

References

Andreae, M. O. and Crutzen, P. J.: Atmospheric Aerosols: Biogeochemical Sources and Role in Atmospheric Chemistry, Science, 276, 1052-1058, 1997.

Andres, R. J. and Kasgnoc, A. D.: A time-averaged inventory of subaerial volcanic sulfur emissions, J. Geophys. Res., 103, D19, 25251-25261, 1998.

Andrews, T., Forster, P. M., Boucher, O., Bellouin, N., and Jones, A.: Precipitation, radiative forcing and global temperature change, Geophys. Res. Lett., 37, L14701, doi:10.1029/2010GL043991, 2010.

Bellouin, N., Boucher, O., Haywood, J., Johnson, C., Jones, A., Rae, J., and Woodward, S.: Improved representation of aerosols for HadGEM2, Technical Note 73, Hadley Centre, Met Office, Exeter, UK, 2007.

Bellouin, N., Rae, J., Jones, A., Johnson, C., Haywood, J., and Boucher, O.: Aerosol forcing in the Climate Model Intercomparison Project (CMIP5) simulations by HadGEM2-ES and the role of ammonium nitrate, J. Geophys. Res., 116, D20206, doi:10.1029/2011JD016074, 2011.

Bollasina, A. M., Ming, Y., and Ramaswamy, V.: Anthropogenic Aerosols and the Weakening of the South Asian Summer Monsoon, Science, 334, 502-505, 2011.

Booth, B., Dunstone, N. J., Halloran, P. R., Andrews, T., and Bellouin, N.: Aerosols implicated as a prime driver of twentieth-century North Atlantic climate variability, Nature, 484, 228-232, doi:10.1038/nature10946, 2012.

Boucher, O., Randall, D., Artaxo, P., Bretherton, C., Feingold, G., Forster, P., Kerminen, V.-M., Kondo, Y., Liao, H., Lohmann, U., Rasch, P., Satheesh, S. K., Sherwood, S., Stevens, B., and Zhang, X. Y.: Clouds and Aerosols. In: Climate Change 2013: The Physical Science Basis. Contribution of Working Group I to the Fifth Assessment Report of the Intergovernmental Panel on Climate Change [Stocker, T. F., Qin, D., Plattner, G.-K., Tignor, M., Allen, S. K., Boschung, J., Nauels, A., Xia, Y., Bex, V., and Midgley, P. M. (eds.)], Cambridge University Press, Cambridge, United Kingdom and New York, NY, USA, 2013.

Chand, D., Wood, R., Anderson, T. L., Satheesh, S. K., and Charlson, R. J.: Satellite derived direct radiative effect of aerosols dependent on cloud cover, Nature Geosci., 2, 181–184, 2009.

Chýlek, P. and Coakley, J. A. Jr.: Aerosol and climate, Science, 183, 75-77, 1974.

Cionni, I., Eyring, V., Lamarque, J. F., Randel, W. J., Stevenson, D. S., Wu, F., Bodeker, G. E., Shepherd, T. G., Shindell, D. T., and Waugh, D. W.: Ozone database in support of CMIP5 simulations: results and corresponding radiative forcing, Atmos. Chem. Phys., 11, 11267-11292, doi:10.5194/acp-11-11267-2011, 2011.

Derwent, R. G., Collins, W. J., Jenkin, M. E., Johnson, C. E., and Stevenson, D. S.: The global distribution of secondary particulate matter in a 3D Lagrangian chemistry transport model, J. Atmos. Chem., 44, 57–95, 2003.

Dong, B., Sutton, R. T., Highwood, E., and Wilcox, L.: The Impacts of European and Asian Anthropogenic Sulfur Dioxide Emissions on Sahel Rainfall, J. Climate, 27, 7000–7017, doi:10.1175/JCLI-D-13-00769.1, 2014.

Flato, G., Marotzke, J., Abiodun, B., Braconnot, P., Chou, S. C., Collins, W., Cox, P., Driouech, F., Emori, S., Eyring, V., Forest, C., Gleckler, P., Guilyardi, E., Jakob, C., Kattsov, V., Reason, C., and Rummukainen, M.: Evaluation of Climate Models. In: Climate Change 2013: The Physical Science Basis. Contribution of Working Group I to the Fifth Assessment Report of the Intergovernmental Panel on Climate Change [Stocker, T. F., Qin, D., Plattner, G.-K., Tignor, M., Allen, S. K., Boschung, J., Nauels, A., Xia, Y., Bex, V., and Midgley, P. M. (eds.)], Cambridge University Press, Cambridge, United Kingdom and New York, NY, USA, 2013.

Gregory, J. M., Ingram, W. J., Palmer, M. A., Jones, G. S., Stott, P. A., Thorpe, R. B., Lowe, J. A., Johns, T. C., and Williams, K. D.: A new method for diagnosing radiative forcing and climate sensitivity, Geophys. Res. Lett., 31, L03205, doi:10.1029/2003GL018747, 2004.

Hansen, J., Sato, M., Ruedy, R., Nazarenko, L., Lacis, A., Schmidt, G. A., Russell, G., Aleinov, I., Bauer, M., Bauer, S., Bell, N., Cairns, B., Canuto, V., Chandler, M., Cheng, Y., Del Genio, A., Faluvegi, G., Fleming, E., Friend, A., Hall, T., Jackman, C., Kelley, M., Kiang, N., Koch, D., Lean, J., Lerner, J., Lo, K., Menon, S., Miller, R., Minnis, P., Novakov, T., Oinas, V., Perlwitz, Ja., Perlwitz, Ju., Rind, D., Romanou, A., Shindell, D., Stone, P., Sun, S., Tausnev, N., Thresher, D., Wielicki, B., Wong, T., Yao, M., and Zhang, S.: Efficacy of climate forcings, J. Geophys. Res., 110, D18104, doi:10.1029/2005JD005776, 2005.

Hemispheric Transport of Air Pollution (HTAP): Hemispheric Transport of Air Pollution 2010. Part A: Ozone and Particulate Matter, Air Pollution Studies No. 17, [Dentener, F., Keating, T., and Akimoto, H. (eds.)], United Nations, New York, 2010.

Holben, B. N., Tanré, D., Smirnov, A., Eck, T. F., Slutsker, I., Abuhassan, N., Newcomb, W. W., Schafer, J. S., Chatenet, B., Lavenu, F., Kaufman, Y. J., Vande Castle, J., Setzer, A., Markham, B., Clark, D., Frouin, R., Halthore, R., Karneli, A., O'Neill, N. T., Pietras, C., Pinker, R. T., Voss, K., and Zibordi, G.: An emerging ground-based aerosol climatology: Aerosol optical depth from AERONET, J. Geophys. Res., 106(D11), 12067–12097, doi:10.1029/2001JD900014, 2001.

Hunke, E. C. and Lipscombe, W. H.: CICE: the Los Alamos sea ice model documentation and software user's manual, Version 4.0, LA-CC-06-012, Los Alamos National Laboratory, New Mexico, 2008.

Hwang, Y.-T., Frierson, D. M. W., and Kang, S. M.: Anthropogenic sulfate aerosol and the southward shift of tropical precipitation in the late 20th century, Geophys. Res. Lett., 40, doi:10.1002/grl.50502, 2013.

Jones, A., Roberts, D. L., Woodage, M. J., and Johnson, C. E.: Indirect sulphate aerosol forcing in a climate model with an interactive sulphur cycle, J. Geophys. Res., 106, 20293–20310, 2001.

Kinne, S., Schulz, M., Textor, C., Guibert, S., Balkanski, Y., Bauer, S. E., Berntsen, T., Berglen, T. F., Boucher, O., Chin, M., Collins, W., Dentener, F., Diehl, T., Easter, R., Feichter, J., Fillmore, D., Ghan, S., Ginoux, P., Gong, S., Grini, A., Hendricks, J., Herzog, M., Horowitz, L., Isaksen, I., Iversen, T., Kirkevåg, A., Kloster, S., Koch, D., Kristjansson, J. E., Krol, M., Lauer, A., Lamarque, J. F., Lesins, G., Liu, X., Lohmann, U., Montanaro, V., Myhre, G., Penner, J., Pitari, G., Reddy, S., Seland, O., Stier, P., Takemura, T., and Tie, X.: An AeroCom initial assessment – optical properties in aerosol component modules of global models, Atmos. Chem. Phys., 6, 1815-1834, doi:10.5194/acp-6-1815-2006, 2006.

Goto, D., Nakajima, T., Dai, T., Takemura, T., Kajino, M., Matsui, H., Takami, A., Hatakeyama, S., Sugimoto, N., Shimizu, A., and Ohara, T.: An evaluation of simulated particulate sulfate over East Asia through global model intercomparison, J. Geophys. Res. Atmos., 120, doi:10.1002/2014JD021693, 2015.

Kahn, R. A., Gaitley, B. J., Garay, M. J., Diner, D. J., Eck, T. F., Smirnov, A., and Holben, B. N.: Multiangle Imaging SpectroRadiometer global aerosol product assessment by comparison with the Aerosol Robotic Network, J. Geophys. Res., 115, D23209, doi:10.1029/2010JD014601, 2010.

Koch, D., Schmidt, G. A., and Field, C. V.: Sulfur, sea salt and radionuclide aerosols in GISS ModelE, J. Geophys. Res., 111, doi:10.1029/2004JD005550, 2006.

Koch, D., Bauer, S., Del Genio, A., Faluvegi, G., McConnell, J. R., Menon, S., Miller, R. L., Rind, D., Ruedy, R., Schmidt, G. A., and Shindell, D.: Coupled aerosol-chemistry-climate twentieth century transient model investigation: Trends in short-lived species and climate responses, J. Climate, 24, 2693–2714, doi:10.1175/2011JCLI3582.1, 2011.

Lamarque, J.-F., Bond, T. C., Eyring, V., Granier, C., Heil, A., Klimont, Z., Lee, D., Liousse, C., Mieville, A., Owen, B., Schultz, M. G., Shindell, D., Smith, S. J., Stehfest, E., Van Aardenne, J., Cooper, O. R., Kainuma, M., Mahowald, N., McConnell, J. R., Naik, V., Riahi, K., and van Vuuren, D. P.: Historical (1850–2000) gridded anthropogenic and biomass burning emissions of reactive gases and aerosols: methodology and application, Atmos. Chem. Phys., 10, 7017-7039, doi:10.5194/acp-10-7017-2010, 2010.

Lawrence, D.M., Oleson, K. W., Flanner, M. G., Thornton, P. E., Swenson, S. C., Lawrence, P. J., Zeng, X., Yang, Z.-L., Levis, S., Sakaguchi, K., Bonan, G. B., and Slater, A. G.: Parameterization improvements and functional and structural advances in version 4 of the Community Land Model, J. Adv. Model. Earth Sys., 3, DOI: 10.1029/2011MS000045, 2011.

Levy, R. C., Mattoo, S., Munchak, L. A., Remer, L. A., Sayer, A. M., Patadia, F., and Hsu, N. C.: The Collection 6 MODIS aerosol products over land and ocean, Atmos. Meas. Tech., 6, 2989-3034, doi:10.5194/amt-6-2989-2013, 2013.

Liu, X., Easter, R. C., Ghan, S., Zaveri, R., Rasch, P., Shi, X., Lamarque, J.-F., Gettelman, A., Morrison, H., Vitt, F., Conley, A., Park, S., Neale, R., Hannay, C., Ekman, A. M. L., Hess, P., Mahowald, N, Collins, W., Iacono, M. J., Bretherton, C. S., Flanner, M. G., and Mitchell, D., Toward a Minimal Representation of Aerosol Direct and Indirect Effects: Model Description and Evaluation, GeoSci. Mod. Dev., 5, 709-739, doi:10.5194/gmd-5-709-2012, 2012.

Madec, G.: NEMO ocean engine, Institut Piere-Simon Laplace (IPSL), France, No. 27, ISSN No. 1288–1619, 2008.

Malm, W. C., Sisler, J. F., Huffman, D., Eldred, R. A., and Cahill, T. A.: Spatial and seasonal trends in particle concentration and optical extinction in the United States, J. Geophys. Res., 99, 1347–1370, 1994.

Meehl, G. A., Washington, W. M., Arblaster, J. M., Hu, A., Teng, H., Kay, J. E., Gettleman, A., Lawrence, D. M., Sanderson, B. M., and Strand, W. G.: Climate Change Projections in CESM1(CAM5) Compared to CCMS4, Journal of Climate, 26, 6287-6308, 2013.

Menon, S., Koch, D., Beig, G., Sahu, S., Fasullo, J., and Orlikowski, D.: Black carbon aerosols and the third polar ice cap, Atmos. Chem. Phys., 10, 4559–4571, 2010.

Miller, R. L., Schmidt, G. A., Nazarenko, L. S., Tausnev, N., Bauer, S. E., Del Genio, A. D., Kelley, M., Lo, K. K., Ruedy, R., Shindell, D. T., Aleinov, I., Bauer, M., Bleck, R., Canuto, V., Chen, Y.-H., Cheng, Y., Clune, T. L., Faluvegi, G., Hansen, J. E., Healy, R. J., Kiang, N. Y., Koch, D., Lacis, A. A., LeGrande, A. N., Lerner, J., Menon, S., Oinas, V., Pérez García-Pando, C., Perlwitz, J. P., Puma, M. J., Rind, D., Romanou, A., Russell, G. L., Sato, M., Sun, S., Tsigaridis, K., Unger, N., Voulgarakis, A., Yao, M.-S., and Zhang, J.: CMIP5 historical simulations (1850-2012) with GISS ModelE2, J. Adv. Model. Earth Syst., 6, no. 2, 441-477, doi:10.1002/2013MS000266, 2014.

Myhre, G., Samset, B. H., Schulz, M., Balkanski, Y., Bauer, S., Berntsen, T. K., Bian, H., Bellouin, N., Chin, M., Diehl, T., Easter, R. C., Feichter, J., Ghan, S. J., Hauglustaine, D., Iversen, T., Kinne, S., Kirkevåg, A., Lamarque, J.-F., Lin, G., Liu, X., Lund, M. T., Luo, G., Ma, X., van Noije, T., Penner, J. E., Rasch, P. J., Ruiz, A., Seland, Ø., Skeie, R. B., Stier, P., Takemura, T., Tsigaridis, K., Wang, P., Wang, Z., Xu, L., Yu, H., Yu, F., Yoon, J.-H., Zhang, K., Zhang, H., and Zhou, C.: Radiative forcing of the direct aerosol effect from AeroCom Phase II simulations, Atmos. Chem. Phys., 13, 1853-1877, doi:10.5194/acp-13-1853-2013, 2013a.

Myhre, G., Shindell, D., Breon, F.-M., Collins, W., Fuglestvedt, J., Huang, J., Koch, D., Lamarque, J.-F., Lee, D., Mendoza, B., Nakajima, T., Robock, A., Stephens, G., Takemura, T., and Zhang, H.: Anthropogenic and Natural Radiative Forcing. In: Climate Change 2013: The Physical Science Basis. Contribution of Working Group I to the Fifth Assessment Report of the Intergovernmental Panel on Climate Change [Stocker, T. F., Qin, D., Plattner, G.-K., Tignor, M., Allen, S. K., Boschung, J., Nauels, A., Xia, Y., Bex, V., and Midgley, P. M.

(eds.)], Cambridge University Press, Cambridge, United Kingdom and New York, NY, USA, 2013b.

Neale, R. B., Chen, C.-C., Gettleman, A., Lauritzen, P. H., Park, S., Williamson, D. L., Conley, A. J., Garcia, R., Kinnison, D., Lamarque, J.-F., Marsh, D., Mills, M., Smith, A. K., Tilmes, S., Vitt, F., Morrison, H., Cameron-Smith, P., Collins, W. D., Iacono, M. J., Easter, R. C., Ghan, S. J., Liu, X., Rasch, P. J., and Taylor, M. A.: Description of the NCAR Community Atmosphere Model (CAM 5.0), NCAR Technical Note TN-486+STR, National Center for Atmospheric Research, Boulder, Colorado, USA, 2012.

Polson, D., Bollasina, M., Hegerl, G. C., and Wilcox, L. J.: Decreased monsoon precipitation in the Northern Hemisphere due to anthropogenic aerosols, Geophys. Res. Lett., 41, doi:10.1002/2014GL060811, 2014.

Reddy, S., Seland, O., Stier, P., Takemura, T., and Tie, X.: An AeroCom initial assessment – optical properties in aerosol component modules of global models, Atmos. Chem. Phys., 6, 1815-1834, doi:10.5194/acp-6-1815-2006, 2006.

Russell, G. L., Miller, J. R., and Rind, D.: A coupled atmosphere-ocean model for transient climate change, Atmosphere-Ocean, 33(4), 683–730, 1995.

Samset, B. H., Myhre, G., Schulz, M., Balkanski, Y., Bauer, S., Berntsen, T. K., Bian, H., Bellouin, N., Diehl, T., Easter, R. C., Ghan, S. J., Iversen, T., Kinne, S., Kirkevåg, A., Lamarque, J.-F., Lin, G., Liu, X., Penner, J. E., Seland, Ø., Skeie, R. B., Stier, P., Takemura, T., Tsigaridis, K., and Zhang, K.: Black carbon vertical profiles strongly affect its radiative forcing uncertainty, Atmos. Chem. Phys., 13, 2423-2434, doi:10.5194/acp-13-2423-2013, 2013.

Samset et al., in preparation.

Schmidt, G.A., Kelley, M., Nazarenko, L., Ruedy, R., Russell, G. L., Aleinov, I., Bauer, M., Bauer, S. E., Bhat, M. K., Bleck, R., Canuto, V., Chen, Y.-H., Cheng, Y., Clune, T. L., Del Genio, A., de Fainchtein, R., Faluvegi, G., Hansen, J. E., Healy, R. J., Kiang, N. Y., Koch, D., Lacis, A. A., LeGrande, A. N., Lerner, J., Lo, K. K., Matthews, E. E., Menon, S., Miller, R. L., Oinas, V., Oloso, A. O., Perlwitz, J. P., Puma, M. J., Putman, W. M., Rind, D., Romanou, A., Sato, M., Shindell, D. T., Sun, S., Syed, R. A., Tausnev, N., Tsigaridis, K., Unger, N., Voulgarakis, A., Yao, M.-S., and Zhang, J.: Configuration and assessment of the GISS

ModelE2 contributions to the CMIP5 archive, J. Adv. Model. Earth Syst., 6, no. 1, 141-184, doi:10.1002/2013MS000265, 2014.

Schulz, M., Textor, C., Kinne, S., Balkanski, Y., Bauer, S., Berntsen, T., Berglen, T., Boucher, O., Dentener, F., Guibert, S., Isaksen, I. S. A., Iversen, T., Koch, D., Kirkevåg, A., Liu, X., Montanaro, V., Myhre, G., Penner, J. E., Pitari, G., Reddy, S., Seland, Ø., Stier, P., and Takemura, T.: Radiative forcing by aerosols as derived from the AeroCom present-day and pre-industrial simulations, Atmos. Chem. Phys., 6, 5225-5246, doi:10.5194/acp-6-5225-2006, 2006.

Shindell, D. T.: Evaluation of the absolute regional temperature potential, Atmospheric Chemistry and Physics, 12, 7955-7960, doi:10.5194/acp-12-7955-2012, 2012.

Shindell, D. and Faluvegi, G.: Climate response to regional radiative forcing during the 20th century, Nat. Geosci., 2, 294-300, 2009.

Shindell, D., Schulz, M., Ming, Y., Takemura, T., Faluvegi, G., and Ramaswamy, V.: Spatial scales of climate response to inhomogeneous radiative forcing, J. Geophys. Res., 115, D19110, doi:10.1029/2010JD014108, 2010.

Shindell, D. T., Voulgarakis, A., Faluvegi, G., and Milly, G.: Precipitation response to regional radiative forcing, Atmos. Chem. Phys., 12, 6969–6982, 2012.

Shindell, D. T., Lamarque, J.-F., Schulz, M., Flanner, M., Jiao, C., Chin, M., Young, P. J., Lee, Y. H., Rotstayn, L., Mahowald, N., Milly, G., Faluvegi, G., Balkanski, Y., Collins, W. J., Conley, A. J., Dalsoren, S., Easter, R., Ghan, S., Horowitz, L., Liu, X., Myhre, G., Nagashima, T., Naik, V., Rumbold, S. T., Skeie, R., Sudo, K., Szopa, S., Takemura, T., Voulgarakis, A., Yoon, J.-H., and Lo, F.: Radiative forcing in the ACCMIP historical and future climate simulations, Atmos. Chem. Phys., 13, 2939-2974, doi:10.5194/acp-13-2939-2013, 2013a.

Shindell, D. T., Pechony, O., Voulgarakis, A., Faluvegi, G., Nazarenko, L., Lamarque, J.-F., Bowman, K., Milly, G., Kovari, B., Ruedy, R., and Schmidt, G.: Interactive ozone and methane chemistry in GISS-E2 historical and future climate simulations, Atmos. Chem. Phys., 13, 2653-2689, doi:10.5194/acp-13-2653-2013, 2013b.

Shindell, D. T., Faluvegi, G., Rotstayn, L., and Milly, G.: Spatial patterns of radiative forcing and surface temperature response, J. Geophys. Res. Atmos., 120, doi:10.1002/2014JD022752, 2015

Smith, S. J., van Aardenne, J., Klimont, Z., Andres, R. J., Volke, A., and Delgado Arias, S.: Anthropogenic sulfur dioxide emissions: 1850–2005, Atmos. Chem. Phys., 11, 1101-1116, doi:10.5194/acp-11-1101-2011, 2011.

Taylor, K. E., Stouffer, R. J., and Meehl, G. A.: An Overview of CMIP5 and the Experiment Design, Bull. Amer. Meteor. Soc., 93, 485–498, doi:10.1175/BAMS-D-11-00094.1, 2012.

Teng, H., Washington, W. M., Branstator, G., Meehl, G. A., and Lamarque, J.-F.: Potential impacts of Asian carbon aerosols on future US warming, Geophys. Res. Lett., 39, L11703, doi:10.1029/2012GL051723, 2012.

Textor, C., Schulz, M., Guibert, S., Kinne, S., Balkanski, Y., Bauer, S., Berntsen, T., Berglen, T., Boucher, O., Chin, M., Dentener, F., Diehl, T., Easter, R., Feichter, H., Fillmore, D., Ghan, S., Ginoux, P., Gong, S., Grini, A., Hendricks, J., Horowitz, L., Huang, P., Isaksen, I., Iversen, I., Kloster, S., Koch, D., Kirkevåg, A., Kristjansson, J. E., Krol, M., Lauer, A., Lamarque, J. F., Liu, X., Montanaro, V., Myhre, G., Penner, J., Pitari, G., Reddy, S., Seland, Ø., Stier, P., Takemura, T., and Tie, X.: Analysis and quantification of the diversities of aerosol life cycles within AeroCom, Atmos. Chem. Phys., 6, 1777-1813, doi:10.5194/acp-6-1777-2006, 2006.

Tilmes, S., Lamarque, J.-F., Emmons, L. K., Kinnison, D. E., Ma, P.-L., Liu, X., Ghan, S., Bardeen, C., Arnold, S., Deeter, M., Vitt, F., Ryerson, T., Elkins, J. W., Moore, F., and Spackman, R.: Description and evaluation of tropospheric chemistry and aerosols in the Community Earth System Model (CESM1.2), Geosci. Model Dev., 8, 1395-1426, doi:10.5194/gmd-8-1395-2015, 2015.

Vet, R., Artz, R. S., Carou, S., Shaw, M., Ro, C.-U., Aas, W., Baker, A., Bowersox, V. C., Dentener, F., Galy-Lacaux, C., Hou, A., Pienaar, J. J., Gillett, R., Forti, M. C., Gromov, S., Hara, H., Khodzher, T., Mahowald, N. M., Nickovic, S., Rao, P. S. P., and Reid, N. W.: A global assessment of precipitation chemistry and deposition of sulfur, nitrogen, sea salt, base cations, organic acids, acidity and pH, and phosphorus, Atmospheric Environment, 93, 3-100, doi:10.1016/j.atmosenv.2013.10.060, 2014.

Voulgarakis, A., and Shindell, D. T., Constraining the sensitivity of regional climate with the use of historical observations. J. Climate, 23, 6068-6073, doi:10.1175/2010JCLI3623.1, 2010.

Walters, D. N., Williams, K. D., Boutle, I. A., Bushell, A. C., Edwards, J. M., Field, P. R., Lock, A. P., Morcrette, C. J., Stratton, R. A., Wilkinson, J. M., Willett, M. R., Bellouin, N., Bodas-Salcedo, A., Brooks, M. E., Copsey, D., Earnshaw, P. D., Hardiman, S. C., Harris, C. M., Levine, R. C., MacLachlan, C., Manners, J. C., Martin, G. M., Milton, S. F., Palmer, M. D., Roberts, M. J., Rodríguez, J. M., Tennant, W. J., and Vidale, P. L.: The Met Office Unified Model Global Atmosphere 4.0 and JULES Global Land 4.0 configurations, Geosci. Model Dev., 7, 361-386, doi:10.5194/gmd-7-361-2014, 2014.

Wilcox, L. J., Highwood, E. J., and Dunstone, N. J.: The influence of anthropogenic aerosol on multi-decadal variations of historical global climate Environ. Res. Lett., 8, 024033, 2013.

Wilcox, L. J., Highwood, E. J., Booth, B. B. B., and Carslaw, K. S.: Quantifying sources of inter-model diversity in the cloud albedo effect, Geophys. Res. Lett., 42, 1568–1575, doi:10.1002/2015GL063301, 2015.

Yu, H., Chin, M., West, J. J., Atherton, C. S., Bellouin, N., Bergmann, D., Bey, I., Bian, H., Diehl, T., Forberth, G., Hess, P., Schulz, M., Shindell, D., Takemura, T., and Tan, Q.: A multimodel assessment of the influence of regional anthropogenic emission reductions on aerosol direct radiative forcing and the role of intercontinental transport, J. Geophys. Res., 118, 700-720, doi:10.1029/2012JD018148, 2013.

Zhang, X. Y., Wang, Y. Q., Niu, T., Zhang, X. C., Gong, S. L., Zhang, Y. M., and Sun, J. Y.: Atmospheric aerosol compositions in China: spatial/temporal variability, chemical signature, regional haze distribution and comparisons with global aerosols, Atmos. Chem. Phys., 12, 779-799, doi:10.5194/acp-12-779-2012, 2012.

Atmos. Chem. Phys. Discuss., doi:10.5194/acp-2015-1017, 2016
Manuscript under review for journal Atmos. Chem. Phys.
Published: 18 January 2016

Atmospheric Chemistry and Physics Discussions
Open Access
EGU

		HadGEM3-GA4			GISS-E2			CESM1		
		Con	Ch0	Ch0-Con	Con	Ch0	Ch0-Con	Con	Ch0	Ch0-Con
Global	Total SO2 (Tg)	0.6370	0.5917	**-0.0453**	1.1511	1.0753	**-0.0758**	-	-	-
	Total SO4 (Tg)	1.5689	1.4993	**-0.0696**	1.0907	1.0142	**-0.0765**	1.4594	1.3234	**-0.1360**
	Mean AOD	0.21692	0.21272	**-0.00420**	0.13122	0.13090	**-0.00032**	0.12336	0.12208	**-0.00128**
	Mean TOA SW (Wm^{-2})	242.274	242.553	**0.279**	241.030	240.996	**-0.034**	236.678	236.864	**0.186**
	Mean temp (K)	289.677	289.791	**0.114**	288.987	288.959	**-0.028**	288.047	288.102	**0.054**
	Δ AOD/Δ SO4 (Tg^{-1})			**0.0603**			**0.00418**			**0.00941**
	Δ TOA SW/Δ AOD ($W\ m^{-2}$)			**-66.443**			**(+)105.723**			**-144.961**
100-120E, 20-40N	Total SO4 (Tg)	0.050229	0.015419	**-0.034810**	0.042600	0.026605	**-0.015995**	0.054137	0.015172	**-0.038965**
	Mean AOD	0.57565	0.28904	**-0.28661**	0.23156	0.18459	**-0.04697**	0.22705	0.15071	**-0.07634**
	Mean TOA SW ($W\ m^{-2}$)	228.828	234.171	**5.343**	233.319	234.224	**0.905**	224.160	228.355	**4.195**
	Mean temp (K)	288.687	289.095	**0.407**	288.965	289.014	**0.049**	289.110	289.404	**0.294**
	Δ AOD/ Δ SO4 (Tg^{-1})			**8.23**			**2.94**			**1.96**
	Δ TOA SW/Δ AOD ($W\ m^{-2}$)			**-18.642**			**-19.268**			**-54.952**

1

Atmos. Chem. Phys. Discuss., doi:10.5194/acp-2015-1017, 2016
Manuscript under review for journal Atmos. Chem. Phys.
Published: 18 January 2016

Atmospheric Chemistry and Physics Discussions

Table 1: Area-integrated SO_2 and SO_4 burdens, area-weighted means of AOD, net down all-sky TOA SW flux, and surface temperature, and ratios of mean change in TOA SW to change in SO_4 burden and change in AOD, for the globe and the region 100°E - 120°E, 20°N - 40°N. Values are shown for each model for the control simulation (Con), the simulation with no SO_2 emissions from China (Ch0), and the difference (Ch0 – Con). AOD is diagnosed for clear-sky conditions in HadGEM3-GA4 and GISS-E2, and for all-sky conditions in CESM1. Global SO_2 burden was calculated only for HadGEM3-GA4 and GISS-E2.

Atmos. Chem. Phys. Discuss., doi:10.5194/acp-2015-1017, 2016
Manuscript under review for journal Atmos. Chem. Phys.
Published: 18 January 2016

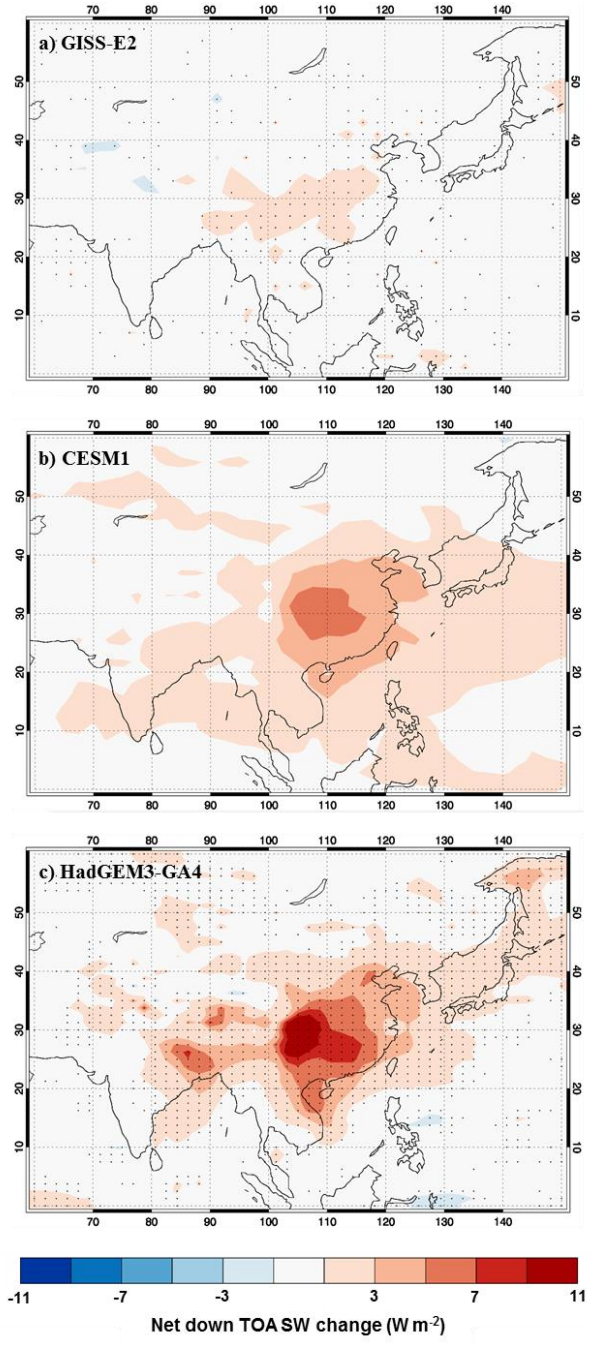

Figure 1: Change in net down TOA SW flux due to removal of SO_2 emissions over China for a) GISS-E2, b) CESM1, and c) HadGEM3-GA4. Differences are calculated as the 150-year

Atmos. Chem. Phys. Discuss., doi:10.5194/acp-2015-1017, 2016
Manuscript under review for journal Atmos. Chem. Phys.
Published: 18 January 2016

Atmospheric Chemistry and Physics Discussions

mean of the perturbation simulation minus the 150-year mean of the control. Plots focuses on the Asian region as changes outside this domain were minimal. Stippling for GISS-E2 and HadGEM3-GA4 indicates the change in that grid-box exceeded 2 standard deviations. Significance was not evaluated for CESM1 as multiple 150-year control runs were not available to assess internal variability for this model.

Atmos. Chem. Phys. Discuss., doi:10.5194/acp-2015-1017, 2016
Manuscript under review for journal Atmos. Chem. Phys.
Published: 18 January 2016

Atmospheric Chemistry and Physics Discussions

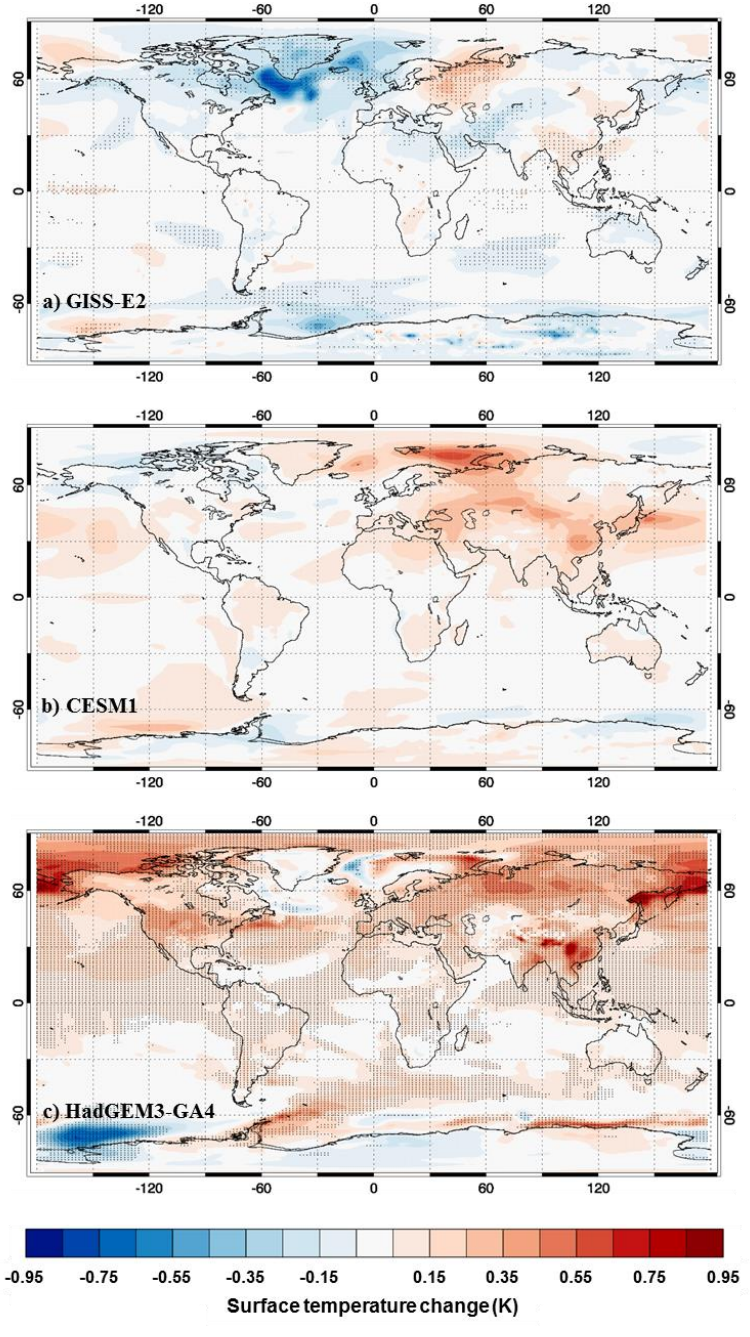

Figure 2: Global changes in surface temperature due to removing SO_2 emissions from China for a) GISS-E2, b) CESM1, and c) HadGEM3. Differences are for 150-year means of

Atmos. Chem. Phys. Discuss., doi:10.5194/acp-2015-1017, 2016
Manuscript under review for journal Atmos. Chem. Phys.
Published: 18 January 2016

perturbation simulation minus control simulation. Stippling for GISS-E2 and HadGEM3-GA4 indicates changes exceeded two standard deviations for that grid box.

Atmos. Chem. Phys. Discuss., doi:10.5194/acp-2015-1017, 2016
Manuscript under review for journal Atmos. Chem. Phys.
Published: 18 January 2016

Atmospheric Chemistry and Physics Discussions

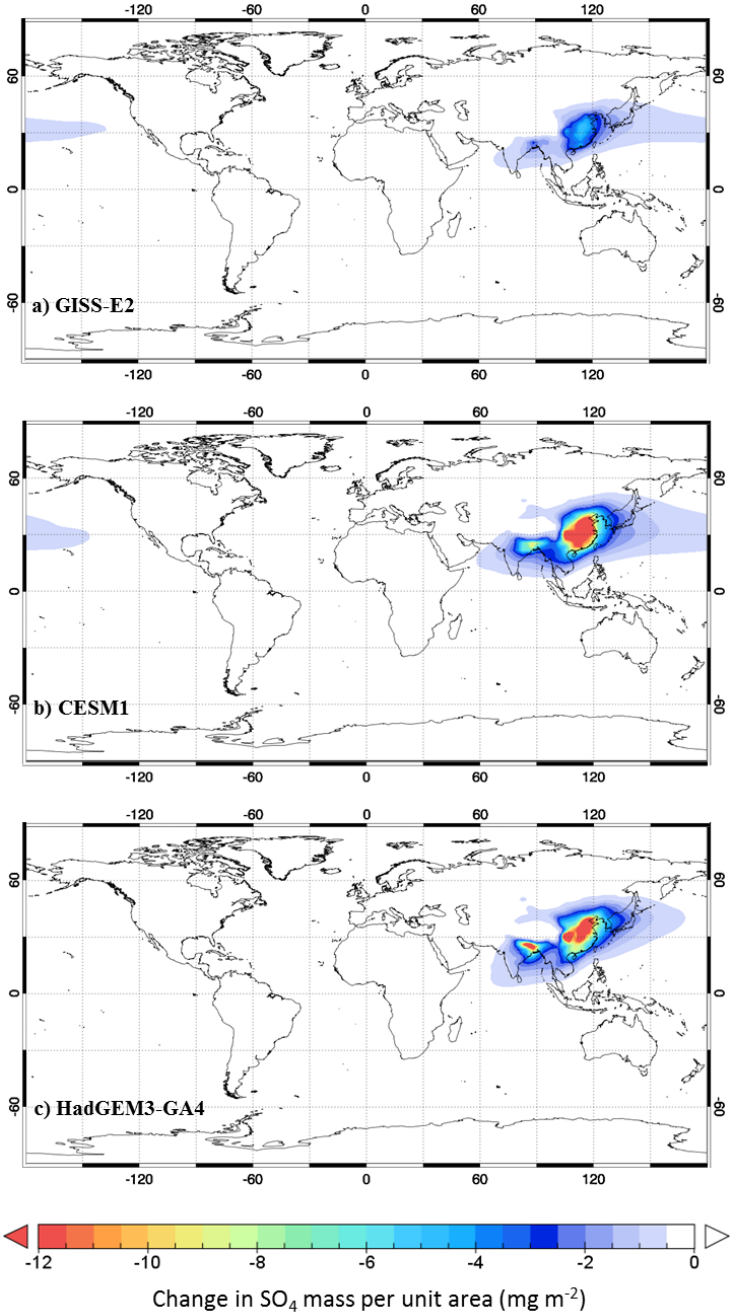

Figure 3: Global changes in column-integrated SO_4 burden due to removing SO_2 emissions from China, for a) GISS-E2, b) CESM1, and c) HadGEM3-GA4. Differences are calculated as perturbation run minus control run, averaged over 150 years.

Atmos. Chem. Phys. Discuss., doi:10.5194/acp-2015-1017, 2016
Manuscript under review for journal Atmos. Chem. Phys.
Published: 18 January 2016

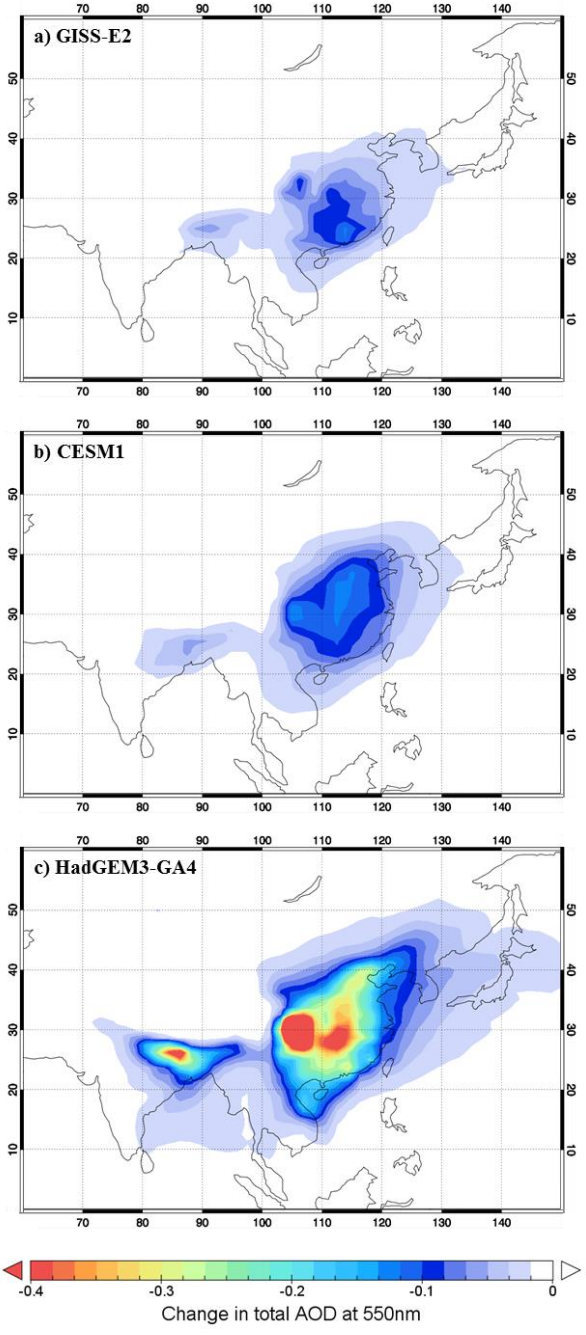

Figure 4: Change in AOD at 550nm due to removing SO_2 emissions from China for a) GISS-E2, b) CESM1, and c) HadGEM3-GA4. For HadGEM3-GA4 and GISS-E2, AOD is calculated for clear-sky conditions, whereas for CESM1 AOD is calculated for all-sky

Atmos. Chem. Phys. Discuss., doi:10.5194/acp-2015-1017, 2016
Manuscript under review for journal Atmos. Chem. Phys.
Published: 18 January 2016

Atmospheric Chemistry and Physics Discussions

conditions, which will generally result in higher values within each simulation. Differences are calculated as perturbation run minus control run, averaged over 150 years. The plot region focuses on Asia as changes outside of this domain were minimal.